Hindawi Publishing Corporation
Science and Technology of Nuclear Installations
Volume 2016, Article ID 6858425, 8 pages
http://dx.doi.org/10.1155/2016/6858425

Research Article

Numerical Investigation of the Transient Behavior of a Hot Gas Duct under Rapid Depressurization

JingBao Liu, ShengYao Jiang, Tao Ma, and RiQiang Duan

Institute of Nuclear and New Energy Technology, Key Laboratory of Advanced Reactor Engineering and Safety of Ministry of Education, Tsinghua University, Beijing 100084, China

Correspondence should be addressed to RiQiang Duan; duanrq@mail.tsinghua.edu.cn

Received 20 October 2015; Revised 9 February 2016; Accepted 17 February 2016

Academic Editor: Alejandro Clausse

A hot gas duct is an indispensable component for the nuclear-process heat applications of the Very-High-Temperature Reactor (VHTR), which has to fulfill three requirements: to withstand high temperature, high pressure, and large pressure transient. In this paper, numerical investigation of pressure transient is performed for a hot gas duct under rapid depressurization. System depressurization imposes an imploding pressure differential on the internal structural elements of a hot gas duct, the structural integrity of which is susceptible to being damaged. Pressure differential and its imposed duration, which are two key factors to evaluate the damage severity of a hot gas duct under depressurization, are examined in regard to depressurization rate and insulation packing tightness. It is revealed that depressurization rate is a decisive parameter for controlling the pressure differential and its duration, whereas insulating-packing tightness has little effect on them.

1. Introduction

A hot gas duct is an indispensable component for nuclear-process heat applications of the Very-High-Temperature Reactors (VHTR), which is on the list of Generation IV initiatives [1, 2]. Heat generated in the reactor core is transferred either to a steam reformer to produce hydrogen and methanol or to an intermediate heat exchanger and a steam gasifier to produce methanol through primary and secondary hot gas ducts, respectively, which are operated at ultra-high temperature and high pressure up to 1100°C and 10 MPa, respectively.

In the design of such a hot gas duct, three requirements have to be fulfilled from the structure and safety viewpoints: to withstand high temperature, high pressure, and large pressure transient. Because of the severe operating conditions and the limitation of the nowadays available materials, a hot gas duct must be thermally insulated to reduce the pressure tubing wall temperature. The typical construction of a hot gas duct is shown in Figure 1, where three zones are formed using three concentric circular tubes. The first zone is the channel between pressure tubing and thermal sleeve, which is tightly packed with fiber-type insulation to reduce the temperature of pressure tubing wall to an accepted value (hereafter, this zone is called the "insulation chamber"). To prevent axial natural or forced convection, fiber-type insulation is axially separated into individual gastight chambers, which are bordered by two ring-shaped manifolds in its two ends. The second zone is the channel between thermal sleeve and hot gas pipe, which is a surge space with a notably smaller gap than the first channel to alleviate pressure shock and protect the structure integrity of hot gas pipe when rapid depressurization occurs (hereafter, this zone is called the "surge channel"). The third zone is hot gas pipe for gas conveyance. To balance the pressure distribution of all interior structural components, two measures are taken in constructing thermal sleeve and hot gas pipe. Thermal sleeve is perforated with pressure-balancing holes at one axial position for each chamber, and hot gas pipe is configured as segments in the same length as one insulation chamber, each of which is separated from its adjacent segments by a narrow breathing clearance to enable the equilibrium of helium pressure between insulation interior and gas medium in hot gas pipe. The breathing clearance should be set as small as possible, only to accommodate the thermal expansion of one segment of hot gas pipe to avoid any extra possibility of thermal convection in

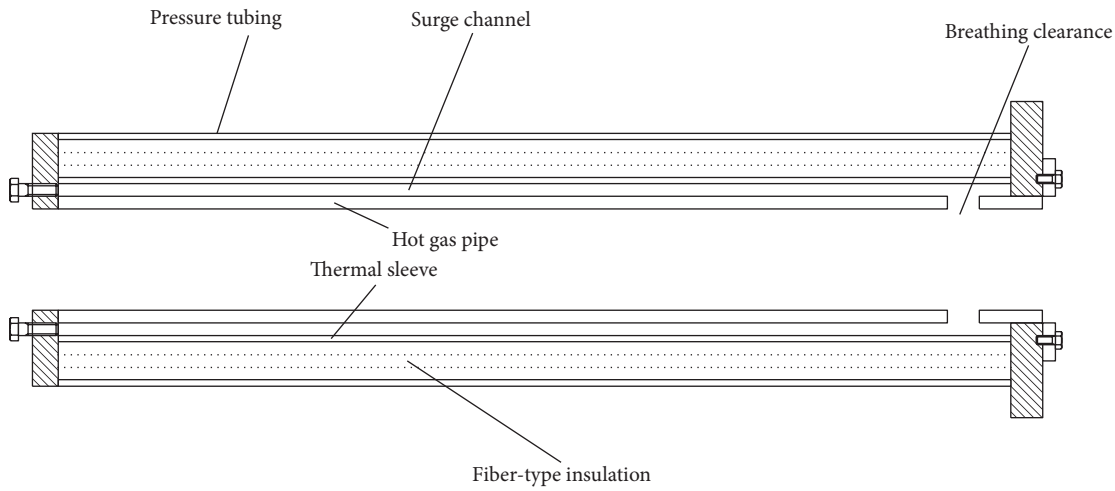

Figure 1: Schematic structure of hot gas duct.

fiber-type insulation. During normal operation, fiber-type insulation material is filled with pressurized helium and is in contact with hot coolant, so no pressure difference appears on the supporting internal structures of fiber-type insulation. Meanwhile pressure tubing remains cold because convection in the insulation chambers is inhibited by stuffed fiber-type insulation. This construction reaches an excellent thermal insulation by screening convection in fiber-type insulation material. However, under a nonsteady situation, such as severe accident of system depressurization, generator trip, or turbomachinery failure, very large pressure transients occur and, consequently, pressure difference appears on the supporting internal structures of fiber-type insulation and thus these elements are subjected to damage and even failure. Due to large flow resistance of fiber-type insulation and flow choking at the pressure-balancing holes and the breathing clearance, pressure differentials among the three zones are however inevitably built up. The damage of internal structural elements is strongly relevant with the built-up pressure differentials and its imposed time period. Thus thermal sleeve and hot gas pipe are subjected to pressure differential at rapid depressurization, which must be evaluated. It is necessary to reveal the relation of pressure stress on thermal sleeve with depressurization rate of the reactor system. Our institute is now beginning a new project to draft the design code for hot gas duct. This study is a preliminary work for that project. The initial step is to develop a numerical code to be able to estimate the above relation.

Weber [3] used a simple one-dimensional model to calculate the pressure transient at rapid depressurization for a hot gas duct with the same structure as that in Figure 1. In his model, a notably simplified calculation of the flow resistance through insulation mats was performed based on a homogeneous and isotropic empirical correlation. Thermal and hydraulic anisotropies of fiber-type insulation were not considered in the model, which significantly affect pressure transient in a hot gas duct.

The goal of this paper is to evaluate the pressure differential that is imposed on thermal sleeve and hot gas pipe at rapid depressurization. Transient analyses for pressure distribution in a hot gas duct are numerically performed after sudden depressurization. The effects of the tightness of fiber-type insulation packing and depressurization rate on pressure differential are numerically investigated. The former is closely related to the technical fabrication of a hot gas duct and is a controlling factor for thermal and hydraulic performances of a hot gas duct. The latter is related to the specification of a hot gas duct, for example, the scale of depressurization which a given hot gas duct can withstand. In this paper, flow behavior in fiber-type insulation is simulated using porous-medium model, which has been well proven in flow simulation through fiber-type insulation.

2. Mathematical Model

In this study, flow through fiber-type insulation material is simulated using the so-called porous-media model [4], where two parameters (permeability and porosity) are introduced in order to consider the field-distributed resistance and the flow anisotropy in fiber-type insulation. Gas flow induced by rapid depressurization is assumed to be an adiabatic process because of its instantaneity. Based on the aforementioned structural characteristics of such a hot gas duct, gas flow is simplified as being symmetrical on the axis of a hot gas duct to save computation resource. Correspondingly, the aperture of pressure-balancing holes on thermal sleeve wall is equivalently modulated. Meanwhile, because of gas tightness in individual insulation chamber, the axial length of computational domain is taken to cover one insulation chamber. The cylindrical coordinate $xr\theta$ is used in the numerical simulation, as shown in Figure 2.

The boundary conditions are set as follows: nonslip wall condition is assumed on the solid boundaries, such as the walls of the pressure tubing, hot gas pipe, thermal sleeve, and two gastight ring-shaped manifolds on the two ends. Gas in the insulation chamber is released through the pressure-balancing holes into the surge channel and subsequently

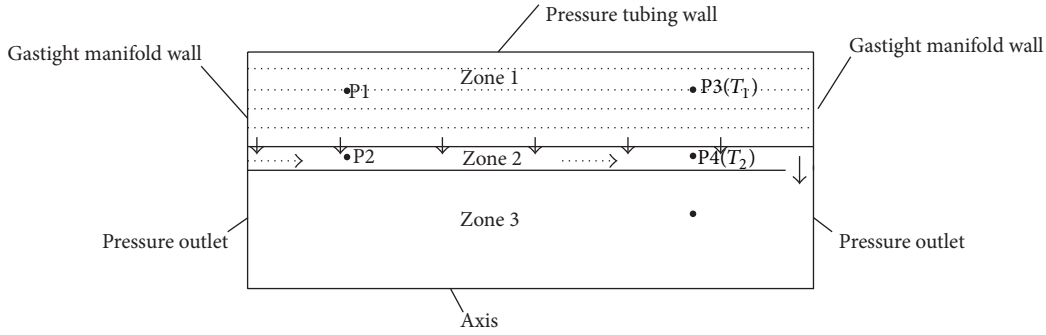

Figure 2: Computational domain.

discharged into the hot gas pipe via the breathing clearance between the two adjacent hot gas pipes.

The depressurization accident of a nuclear plant system manifests itself in its amplitude and response of the system. Based on the hypothetical accidents for helium-cooled reactors [3], the depressurization process of a hot gas pipe can be approximated as an exponential decay function

$$p = p_0 - \Delta p \cdot \left(1 - e^{-t/\tau}\right), \tag{1}$$

where p_0 is the initial pressure in the hot gas pipe, Δp is the total depressurization amplitude, and τ is the time constant of depressurization. The depressurization rate is a time-variable that depends on the depressurization amplitude and time constant.

The governing equations based on the properties per unit volume are expressed in the conservative form as follows.

Continuity equation is shown as follows:

$$\frac{\partial \rho}{\partial t} + \nabla \cdot (\rho \vec{v}) = 0. \tag{2}$$

Regarding the symmetry of the computation domain, the continuity equation can be expanded in cylinder coordinates as

$$\frac{\partial \rho}{\partial t} + \frac{\partial}{\partial x}(\rho v_x) + \frac{\partial}{\partial r}(\rho v_r) + \frac{\rho v_r}{r} = 0, \tag{3}$$

where v_x and v_r are the axial and radial velocities, respectively.

Momentum equation is shown in the following:

$$\frac{\partial}{\partial t}(\rho \vec{v}) + \nabla \cdot (\vec{v} \otimes (\rho \vec{v})) = -\nabla P + \nabla \cdot \bar{\bar{\tau}} + \vec{S}, \tag{4}$$

where p, $\bar{\bar{\tau}}$, and $\vec{S}$ are the static pressure, viscosity stress tensor, and source term that results from the resistance of fiber-type insulation, respectively,

$$\bar{\bar{\tau}} = \mu \left[\left(\nabla \vec{v} + \nabla \vec{v}^T \right) - \frac{2}{3} \nabla \cdot \vec{v} I \right], \tag{5}$$

where μ and I are the dynamic viscosity and unit tensor, respectively. The momentum equation (5) is further expanded in x- and r-coordinate components as follows:

$$\begin{aligned}
&\frac{\partial}{\partial t}(\rho v_x) + \frac{1}{r}\frac{\partial}{\partial x}(r \rho v_x v_x) + \frac{1}{r}\frac{\partial}{\partial r}(r \rho v_r v_x) \\
&\quad = -\frac{\partial p}{\partial x} + \frac{1}{r}\frac{\partial}{\partial x}\left[r\mu \left(2\frac{\partial v_x}{\partial x} - \frac{2}{3}(\nabla \cdot \vec{v}) \right) \right] \\
&\qquad + \frac{1}{r}\frac{\partial}{\partial r}\left[r\mu \left(\frac{\partial v_x}{\partial r} + \frac{\partial v_r}{\partial x} \right) \right] + S_x, \\
&\frac{\partial}{\partial t}(\rho v_r) + \frac{1}{r}\frac{\partial}{\partial x}(r \rho v_x v_r) + \frac{1}{r}\frac{\partial}{\partial r}(r \rho v_r v_r) \\
&\quad = -\frac{\partial p}{\partial r} + \frac{1}{r}\frac{\partial}{\partial x}\left[r\mu \left(\frac{\partial v_r}{\partial x} + \frac{\partial v_x}{\partial r} \right) \right] \\
&\qquad + \frac{1}{r}\frac{\partial}{\partial r}\left[r\mu \left(2\frac{\partial v_r}{\partial r} - \frac{2}{3}(\nabla \cdot \vec{v}) \right) \right] - 2\mu \frac{v_r}{r^2} \\
&\qquad + \frac{2}{3}\frac{\mu}{r}(\nabla \cdot \vec{v}) + S_r.
\end{aligned} \tag{6}$$

The flow resistance through fiber-type insulation is modeled using the porous-media model, which consists of two parts: the *Darcy* viscosity resistance and the inertia resistance, as shown in the following:

$$S_i = -\left(\frac{\mu}{\alpha} v_i + \frac{C_2}{2} \rho |v| v_i \right), \tag{7}$$

where α and C_2 are the permeability of porous medium and the inertia resistance coefficient, respectively. The resistance anisotropy of fiber-type insulation is reflected by the field distribution of these two parameters based on the stuffing scheme of fiber-type insulation.

The permeability of porous medium depends on the size, compactness, and arrangement of fiber, which is calculated using the Jackson correlation [4] as shown in the following:

$$\frac{\alpha}{D_p^{\,2}} = f(\varepsilon), \tag{8}$$

where D_p and ε are the equivalent diameter of fiber and the porosity of fiber packing, respectively.

The inertia resistance coefficient is a function of the porosity and the fiber size, as shown in the following:

$$C_2 = \frac{3.5}{D_p}\frac{(1-\varepsilon)}{\varepsilon^3}. \tag{9}$$

For energy equation, it is assumed that gas medium and fiber-type insulation are in local thermal-homogeneous equilibrium, which implies that there is no heat transfer between gas and fiber-type insulation inside each mesh at numerical computation:

$$\begin{aligned}&\frac{\partial}{\partial t}\left(\varepsilon\rho E_f + (1-\varepsilon)\,\rho_s E_s\right) + \nabla\cdot\left(\vec{v}\left(\rho_f E_f + p\right)\right)\\ &\quad = \nabla\cdot\left(k_{\text{eff}}\nabla T + \left(\overline{\overline{\tau}}_{\text{eff}}\cdot\vec{v}\right)\right),\end{aligned} \tag{10}$$

where E_f is the internal energy of fluid; ρ_s and E_s are the density and specific internal energy of fiber per unit volume, respectively; and k_{eff} is the effective thermal conductivity coefficient, which is the volume-weighted average of gas conductivity k_f and fiber conductivity k_s, as shown in the following:

$$k_{\text{eff}} = \varepsilon k_f + (1-\varepsilon)\,k_s. \tag{11}$$

The gas medium is helium, which is treated as perfect gas with the constant specific heat and the adiabatic exponent κ. The state equations are

$$\begin{aligned}p &= \rho RT,\\ E_f &= \frac{RT}{\kappa - 1},\end{aligned} \tag{12}$$

where R is the gas constant.

3. Numerically Solving Strategy

The pressure-correction method, which was proposed by McGuirk and Page [5], is applied to solve the problem. This method is suitable for calculating flow with a wide range of the Mach number. The hyperbolic nature of the controlling equation system is maintained using a retarded-pressure approach. To preserve the conservative form of the differential equations after space discretization, the selected primary variables are the density, the momentum, and the energy. In the discretization scheme, staggered meshing is applied, where the primary variables and pressure are defined in the center of cells, and the convection terms are defined on the edges of cells. Figure 3 shows the staggered grid system and notation used.

The momentum equations are discretized by integrating over a volume limited by the grid lines numbered with i and $i+1$ in the axial direction and $j-1/2$ and $j+1/2$ in the radial direction. The following shows the discretization strategy of the axial-direction momentum equation, the same of which is adopted for the radial-direction momentum equation. Viscous terms are conventionally written as the central difference scheme. And the source term brought with fiber-insulation is linearized based on the prevailing value of its dependent variable. In the following, the unsteady term and the convection terms are given in detail. The backward Euler implicit scheme is used for discretization of the transient term, as given in

$$\frac{\partial}{\partial t}\left(\rho v_x\right) \sim \frac{1}{\Delta t}\left(\left(\rho v_x\right)_{i+1/2,j} - \left(\rho v_x\right)^0_{i+1/2,j}\right), \tag{13}$$

where

$$\left(\rho v_x\right)_{i+1/2,j} = \frac{\rho_{i,j} + \rho_{i+1,j}}{2}\left(v_x\right)_{i+1/2,j}. \tag{14}$$

For the convection term of the momentum, the convecting velocity at the controlling volume edges is interpolated from its two neighboring cells, as given in

$$\begin{aligned}\left(v_x\right)_{i,j} &= \frac{\left(v_x\right)_{i+1/2,j} + \left(v_x\right)_{i-1/2,j}}{2},\\ \left(v_r\right)_{i+1/2,j-1/2} &= \frac{\left(v_r\right)_{i,j-1/2} + \left(v_r\right)_{i+1,j-1/2}}{2},\end{aligned} \tag{15}$$

and the convective momentum is written using the upwind scheme

$$\begin{aligned}\left(\rho v_x\right)_{i,j} &= \begin{cases}\rho_{i,j}\left(v_x\right)_{i-1/2,j}, & \left(v_x\right)_{i+1/2,j} > 0\\ \rho_{i,j}\left(v_x\right)_{i+1/2,j}, & \left(v_x\right)_{i+1/2,j} < 0,\end{cases}\\ &\left(\rho v_x\right)_{i+1/2,j-1/2}\\ &= \begin{cases}\dfrac{\rho_{i,j-1}+\rho_{i+1,j-1}}{2}\left(v_x\right)_{i+1/2,j-1}, & \left(v_r\right)_{i+1/2,j-1/2} > 0\\ \dfrac{\rho_{i,j-1}+\rho_{i+1,j-1}}{2}\left(v_x\right)_{i+1/2,j}, & \left(v_r\right)_{i+1/2,j-1/2} < 0.\end{cases}\end{aligned} \tag{16}$$

Thus the convection term of the momentum equations is formulated as

$$\begin{aligned}&\frac{1}{r}\frac{\partial}{\partial x}\left(r v_x \rho v_x\right) \sim \frac{1}{\Delta x}\left(\left(v_x\right)_{i+1,j}\left(\rho v_x\right)_{i+1,j}\right.\\ &\qquad \left. - \left(v_x\right)_{i,j}\left(\rho v_x\right)_{i,j}\right),\\ &\frac{1}{r}\frac{\partial}{\partial r}\left(r v_r \rho v_x\right) \sim \frac{1}{\Delta r}\left(\left(v_r\right)_{i+1/2,j+1/2}\left(\rho v_x\right)_{i+1/2,j+1/2}\right.\\ &\qquad \left. - \left(v_r\right)_{i+1/2,j-1/2}\left(\rho v_x\right)_{i+1/2,j-1/2}\right).\end{aligned} \tag{17}$$

4. Results and Discussion

Under the depressurization of a hot gas duct, the thermal sleeve and the hot gas pipe are vulnerable to the damage of structural integrity because they are subjected to imploding pressure stress. In this paper, two parameters are investigated regarding the effect of pressure differentials on the wall of the thermal sleeve and the hot gas pipe. The first parameter is the depressurization rate, which is relevant to the safety specification of a hot gas duct. The actual depressurization

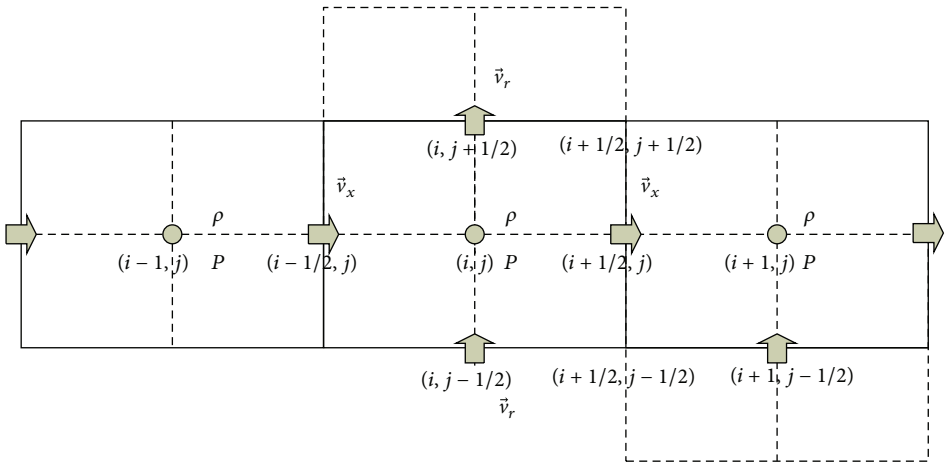

Figure 3: The staggered grid system.

Table 1: Input parameters for numerical simulation.

Symbol	Parameter	Numerical value
p_0	Initial pressure	11 bar
Δp	Depressurization amplitude	1.0~9.6 bar
τ	Time constant of depressurization	0.00181 s
L	Length of insulation	0.88 m
S_0	Cross section of surge channel	0.00755 m^2
V_I	Interior volume of insulation	0.085 m^3
D_h	Hydraulic diameter of surge channel	0.02 m
R	Gas constant for helium	2077.12 J/kg·K
κ	Adiabatic exponent	1.667
T_0	Initial temperature helium	300 K
ξ	Coefficient of friction	0.016
S	Effective aperture of surge channel	0.0018 m^2
S_{IE}	Effective aperture of perforated tube	0.0006 m^2

scenario is that the depressurization rate decays with time, as shown in (1). To be consistent with actual depressurization scenarios, the depressurization rate in this study is featured by moderating its amplitude while maintaining the response time constant. The input parameters for numerical simulation are shown in Table 1, which are consistent with those of the Weber experiments. To track the pressure response to depressurization inside a hot gas duct, pressure transients are sampled in the three zones, where the sample points are arranged as follows: P1 and P3 are in the insulation chamber, P2 and P4 are in the surge channel, and P5 is in the hot gas pipe (shown in Figure 2). The second parameter is the packing tightness in the insulation chamber, which is related to the fabrication of a hot gas duct.

4.1. Effect of the Depressurization Amplitude. The effect of the depressurization rate is investigated by changing the depressurization amplitude from 1 to 9 bar. At first, to verify the validation of the numerical scheme, comparison is made with the Weber experimental data at 9-bar depressurization amplitude [3], which is depicted in Figure 4(d). It is revealed that they are above all in good agreement, except that our calculated pressure transients are in a bit quicker response than that of the Weber experiments.

The pressure transients, which are sampled in the three zones at different depressurization amplitudes, are recorded, shown in Figure 4. The pressure transient response to depressurization in a hot gas pipe is almost instantaneous, the time scale of which is on the order of ten milliseconds. However, the pressure transient response in both the surge channel and insulation chamber is greatly delayed because of choking at the breathing clearance and large flow resistance through fiber-type insulation. And moreover, flow resistance of gas discharge is mainly concentrated on the breathing clearance, where choking is susceptible to being triggered. The inset graphs in Figure 4 show the pressure transient in both the surge channel and the insulation chamber by zooming in for clarity, which demonstrates the pressure distribution in the insulation chamber and the surge channel.

Regarding the damage of structural integrity, the pressure differential and its duration imposed on the supporting interior elements are two key indicators to evaluate the damage severity resulting from depressurization, which are helpful to filter out the most vulnerable elements under depressurization and meanwhile provide the instructions or guidance for design codes of hot gas ducts.

The pressure differentials on the wall of the thermal sleeve and hot gas pipe, which are shown in Figures 5 and 6, respectively, increase with the depressurization amplitude. The wall of the hot gas pipe has to withstand a larger pressure differential, which is approximately 2 orders of magnitude higher than that on the wall of the thermal sleeve. At small depressurization amplitude, such as depressurization amplitude with 3 bar in Figures 5 and 6, the pressure differential rapidly reaches a peak and subsequently gradually decreases with time. Choking may occur at the breathing clearance in the initial stage because of the initial maximum depressurization rate, where the mass flow rate only depends on the upstream pressure in the surge channel. Shortly after, the gas

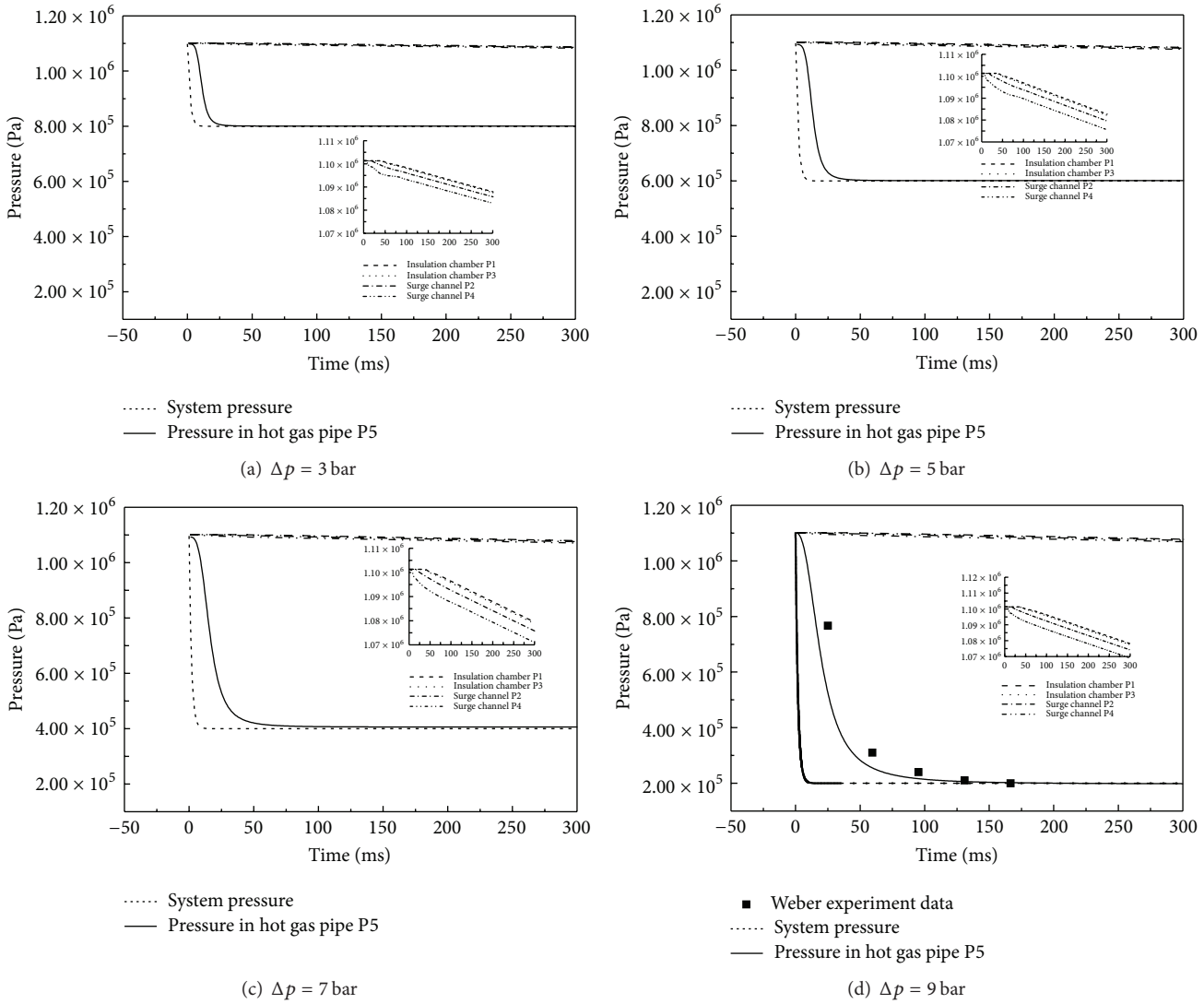

Figure 4: Pressure transient in hot gas duct.

flow decreases and transitions to the subsonic regime, where the mass flow depends on the pressure difference between the surge channel and the hot gas pipe. With an increase in depressurization amplitude, choking at the breathing clearance is held for a longer time when the depressurization amplitude is larger than 3 bar. We examine the gas velocity and mass flow rate at the breathing clearance, the latter of which is shown in Figure 7. The transient of the mass flow rate at the breathing clearance has a similar trend with the pressure differential. Meanwhile, the gas temperature in the insulation chamber is also verified. When the gas discharges into the surge channel during depressurization, the gas temperature slightly decreases because of the transformation of internal energy into the kinetic energy in the range below 0.2°C, as shown in Figure 8. So the temperature effect on gas density and sonic speed can be neglected.

For the imposed duration of pressure differential, the concept of time constant is applied in order to assess it, which reflects the response time inside a hot gas duct to the system depressurization. The time constant is defined as time length when the pressure decrease reaches 63.2% of the total depressurization amplitude, the concept of which is the same as that in linear lumped systems. Table 2 demonstrates the time constants of the three zones for different depressurization amplitudes. The time constant of the hot gas pipe is one order of magnitude higher than that of the system, whereas the time constants of the other two zones are 3 orders of magnitude higher than that of the system. For the effect of the depressurization amplitude on the time constant, it is revealed that the time constant increases with the depressurization amplitude. It is concluded that the more rapid depressurization the system experiences the more larger pressure differential and the longer duration are imposed on the thermal sleeve and the hot gas pipe.

4.2. Effect of Insulation Packing Tightness. Fiber-type insulation packing tightness in an insulation chamber is reflected by the porosity in the porous-media model, whose value

Table 2: Time constant of response for the three zones.

Depressurization amplitude, bar	Maximum depressurization rate, bar/s	System, ms	Hot gas pipe, ms	Surge channel, ms	Insulation chamber, ms
3	1657	1.81	13	3800	4560
5	2762	1.81	14	4213	5417
7	3867	1.81	19	4826	6636
9	4972	1.81	25	6205	7756

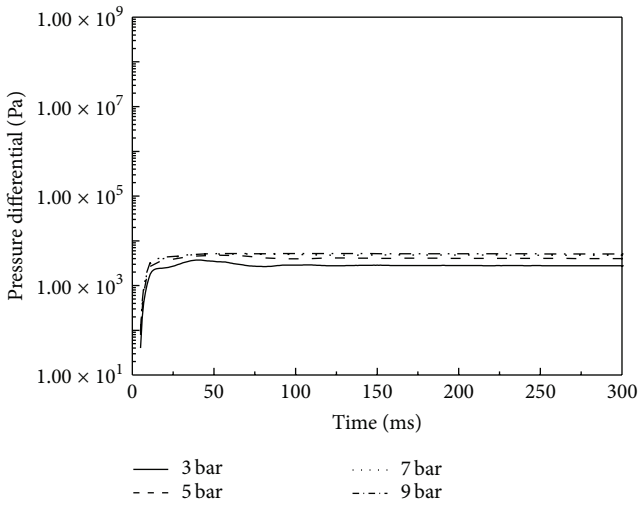

Figure 5: Pressure differential on the wall of thermal sleeve.

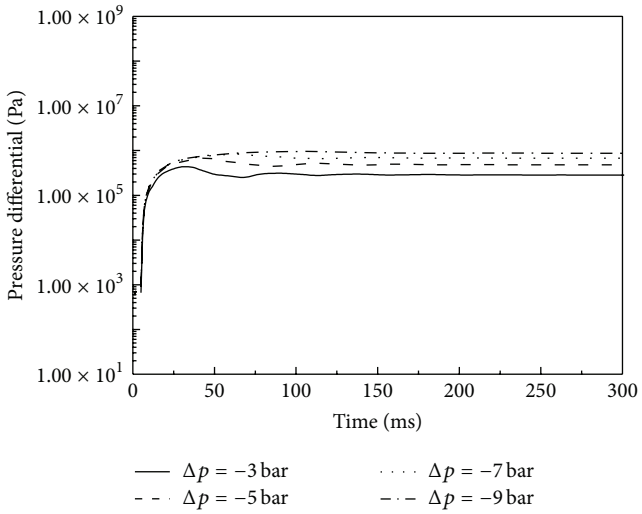

Figure 6: Pressure differential on the wall of hot gas duct.

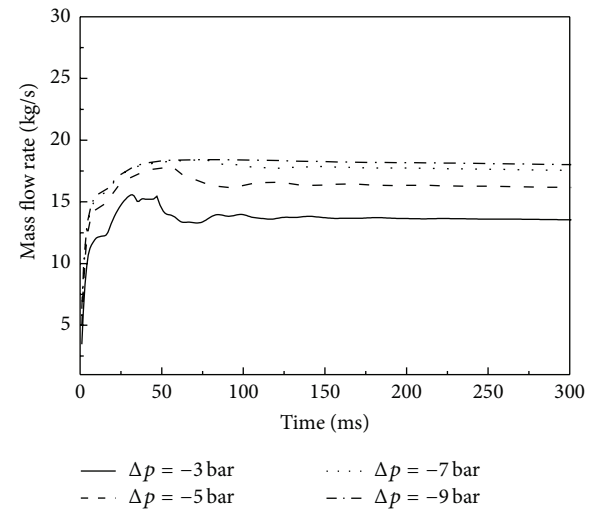

Figure 7: Mass flow rates at the breathing clearance.

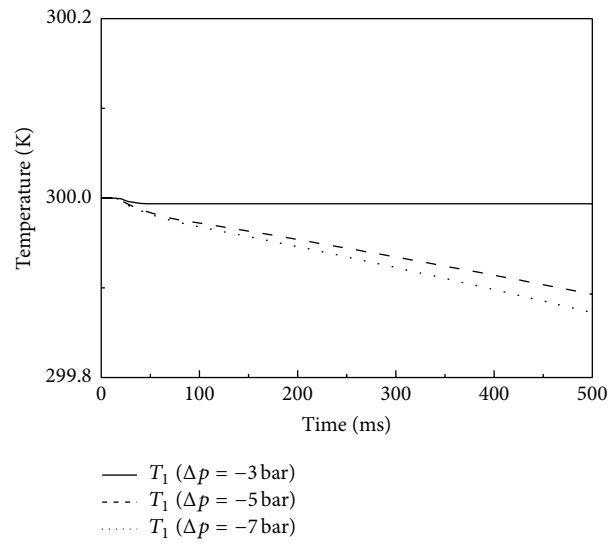

Figure 8: Temperature evolutions in insulation chamber at depressurization process.

is taken from 0.1 to 0.7 in the numerical simulations. It is revealed that the porosity of insulation tightness hardly affects the pressure differential and its duration on the supporting interior elements of the hot gas duct. Figure 9 shows the pressure differentials on the wall of the hot gas pipe under different porosities of fiber-type insulation packing, the curves of which are almost superposed into one curve.

5. Conclusion

Numerical simulations are performed for pressure transient of a hot gas duct under rapid depressurization. Hot gas duct is an indispensable component for the Very-High-Temperature Reactor (VHTR). Regarding the structural integrity of the

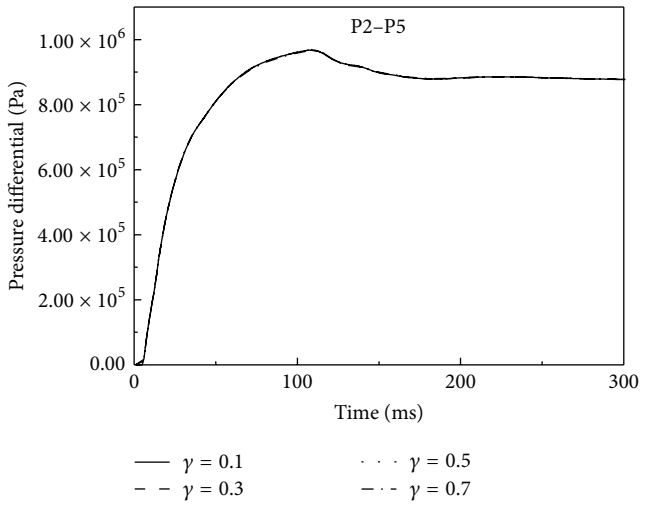

Figure 9: Effect of porosity on pressure differential on the wall of hot gas pipe.

internal structural elements of a hot gas duct, the pressure differential and its imposed duration are two suitable parameters to be able to evaluate the damage severity of a hot gas duct in rapid depressurization accidents. We investigate the following two factors concerned with the effect on the above two parameters. One is the depressurization rate of the system, which reflects the severity of depressurization accidents, and another is fiber-type insulation packing tightness, which is closely relevant to the fabrication of the component. It is shown from the numerical simulations that the pressure differential and its duration are mainly determined by the depressurization rate of the system, and however fiber-type insulation stuffing tightness has little effect on them.

In addition, it should be mentioned that this study is a preliminary work for analyses of the depressurization process of hot gas duct. We have hitherto developed this simulation code and verified it by comparison with the Weber experiments. But its function and modules are still limited. In the future, other modules, such as contour of scalar variables, will be added to it to enrich its functions, as one of reviewers advised.

Competing Interests

The authors declare that there are no competing interests regarding the publication of this paper.

Acknowledgments

This work was supported by the Science Fund for Creative Research Groups of the National Natural Science Foundation of China under Grant nos. 51321002 and 11472155.

References

[1] T. Abram and S. Ion, "Generation-IV nuclear power: a review of the state of the science," *Energy Policy*, vol. 36, no. 12, pp. 4323–4330, 2008.

[2] S. Fujiwara, S. Kasai, H. Yamauchi et al., "Hydrogen production by high temperature electrolysis with nuclear reactor," *Progress in Nuclear Energy*, vol. 50, no. 2–6, pp. 422–426, 2008.

[3] H. Weber, "Investigation on the depressurization behavior of a typical HHT thermal insulation," in *Proceedings of the Specialists' Meeting on Gas-Cooled Reactor Safety and Licensing Aspects*, pp. E154–E162, Lausanne, Switzerland, September 1980.

[4] G. W. Jackson and D. F. James, "The permeability of fibrous porous media," *The Canadian Journal of Chemical Engineering*, vol. 64, no. 3, pp. 364–374, 1986.

[5] J. J. McGuirk and G. J. Page, "Shock capturing using a pressure-correction method," *AIAA Journal*, vol. 28, no. 10, pp. 1751–1757, 1990.